Plasma Phys. Control. Fusion **53** (2011) 014007 (10pp) doi:10.1088/0741-3335/53/1/014007

High efficiency x-ray source based on inverse Compton scattering in an optical Bragg structure

Vadim Karagodsky and Levi Schächter

Department of Electrical Engineering, Technion, Israel Institute of Technology, Haifa 32000, Israel

E-mail: levi@ee.technion.ac.il

Received 31 October 2009, in final form 12 December 2009
Published 16 December 2010
Online at stacks.iop.org/PPCF/53/014007

Abstract

Existing x-ray sources based on inverse Compton scattering rely on free-space lasers and have modest efficiency due to the inherent limitation of maintaining their peak field intensity over a few Rayleigh lengths. Moreover, their typical interaction spots are tens of micrometres in diameter and they rely on large electron accelerators. We propose a new structure that mitigates many of these limiting factors by confining the interaction in an optical Bragg waveguide, specially designed to support a TEM mode within its sub-micrometre hollow core. This allows the e-beam–laser interaction to be as long as the waveguide itself, resulting in superior spectral quality of the emerging x-ray. Furthermore, the regular RF accelerator may be replaced by an optical Bragg accelerator. This two-stage design, from acceleration to x-ray emission, is expected to have a table-top size, and it is estimated to provide x-ray brightness of 3×10^{17} (photons s^{-1} mm^{-2} $mrad^{-2}$/0.1%BW), while utilizing laser power several orders of magnitude smaller than comparable free-space sources.

(Some figures in this article are in colour only in the electronic version)

1. Introduction

X-ray generation has been undergoing a steady revolution for the past five decades. The brightness of these sources, measured in photons s^{-1} mm^{-2} $mrad^{-2}$/0.1%-bandwidth, has been rising exponentially, starting from x-ray tubes (10^7) on to bending magnets (10^{10}–10^{14}), wigglers (10^{13}–10^{16}) and undulators (10^{15}–10^{22}) [1].

X-ray sources based on undulators and wigglers became essential in numerous fields: material science [2], biomedicine [3], chemistry [4], crystallography, solid state physics [5] and many others [1, 6]. In both configurations the mechanism is similar: a relativistic electron beam interacts with a static periodic magnetic field, generated by an array of magnets with interchanging polarity. The magnetic field induces transverse oscillations in the e-beam trajectory, causing a dipole-like radiation to be emitted. Due to relativistic effects, the emitted

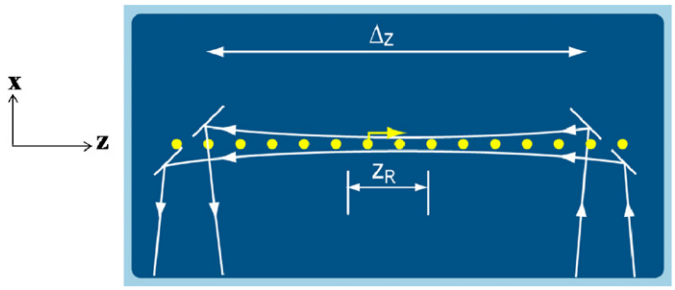

Figure 1. Conventional free-space Compton scattering setup. An interaction between a laser and an e-beam, propagating towards each other, generates x-ray emission in the $+z$ direction. The laser is typically focused to a 10 μm spot, which corresponds to Rayleigh length z_R of the order of millimetres. Δ_z is the overall interaction length.

radiation is Doppler shifted from a microwave into the x-ray region, and the light becomes strongly collimated in front of the e-beam.

A major figure of merit for undulators and wigglers is called the 'deflection parameter':

$$\kappa = \frac{eB\lambda_U}{2\pi m_0 c}; \tag{1}$$

where e and m are the electron charge and mass, respectively, B is the strength of the magnetic field, λ_U is the undulator/wiggler period and c is the speed of light in vacuum. The deflection parameter is a measure of how strongly the e-beam is deflected as a result of the interaction with the magnetic field. In wigglers the magnetic field is stronger than in undulators and the magnets are more widely spaced (λ_U is larger). Accordingly the e-beam deflection is typically much larger than in an undulator and consequently, wiggler-based sources are *less* bright. Optimal deflection parameter for maximal brightness is $\kappa = \sqrt{2}$, and this is approximately where modern undulator-based sources operate. For wigglers the deflection parameter is typically measured in tens. In terms of this deflection parameter κ, and accounting for the double Doppler shift, the wavelength of the emitted radiation is given by

$$\lambda_{\text{x-ray}} = \frac{\lambda_U}{2\gamma^2}\left(1 + \frac{\kappa^2}{2}\right). \tag{2}$$

In equation (2) $\lambda_{\text{x-ray}}$ is the wavelength of the emitted light (x-ray) along the optical axis and γ is the Lorentz relativistic energy factor of the electrons. In order to Doppler shift the light from a microwave (λ_U of at least several centimetres) into x-ray, the e-beam has to be accelerated to gigaelectronvolts (γ in thousands). This requires relatively large and expensive acceleration systems. Another disadvantage is the size of undulators and wigglers themselves—in order to have reasonably monochromatic x-rays, tens to hundreds of magnet periods are required, each several centimetres long. Today, undulators and wigglers are mostly accommodated in national laboratories or national facilities.

In an effort to overcome the stringent (GeV) acceleration requirements of undulators and wigglers, laser-based Compton scattering x-ray experiments have emerged. These sources harness the electromagnetic field of a laser as a replacement for the static magnetic field of an undulator. A typical configuration is a 180° incidence between the e-beam and the laser pulse, as described in figure 1, but 90° and other angles of incidence are also used [7, 8]. For an electromagnetic wiggler $\kappa = eE\lambda_L/2\pi m_0 c^2$ whereas the wavelength of the radiation on

axis is

$$\lambda_{\text{x-ray}} = \frac{\lambda_{\text{L}}}{4\gamma^2}\left(1 + \frac{\kappa^2}{2}\right), \tag{3}$$

E being the amplitude of the electric field and λ_{L} the laser wavelength. Equation (3) assumes head-on (180°) incidence and linear polarization of the laser. Comparing equations (2) and (3) reveals an extra factor of 2 in the relativistic double Doppler shift term $4\gamma^2$, which is due to the fact that the field is no longer static and the laser pulse propagates towards the e-beam. While this factor is in our favour, the main benefit stems from the fact that the laser wavelength λ_{L} is four orders of magnitude smaller than the undulator period λ_{U} and, consequently, the e-beam acceleration energy requirement is reduced by two orders of magnitude from gigaelectronvolts to tens of megaelectronvolts. This is the main advantage of Compton scattering sources over undulators. The deflection parameter of Compton sources is of the order of $\kappa \sim 1$ to the very most [9–11], provided that high-power laser pulses (TW) are used.

The first demonstration of this concept was reported by Carmel *et al* [12] at Naval Research Laboratory. In this demonstration, x-rays were produced by scattering the e-beam from a high-power microwave pulse. In recent years, several groups have reported successful x-ray generation via Compton scattering from a *laser pulse*. In 2000, at the Brookhaven National Laboratory Accelerator Test Facility (BNL ATF) collaborators reported [13] generation of 6.5 keV photons by scattering a 10.6 m CO_2 laser from a 60 MeV e-beam. A collaboration at the Lawrence Livermore National Laboratory, at the PLEIADES facility, demonstrated generation of 78 keV x-ray photons [14] using a 57 MeV e-beam and a 820 nm Ti : sapphire laser. An all-optical setup was reported more recently [10], employing a 800 nm Ti : sapphire laser split into two pulses: one used for the acceleration of electrons (5 MeV) and the second, counter-propagating pulse, used for Compton scattering. The emerging photons were measured to be in the range from 0.4 to 2 keV. In addition to Compton scattering based on e-beams produced by photocathode rf-guns, more elaborate methods of laser back-scattering from relativistic mirrors have been recently proposed. Bulanov *et al* [15] proposed a mechanism for coherent back-scattering of a laser from counter-propagating plasma density spikes, acting as flying parabolic relativistic mirrors, created using short and intense laser pulses. Additionally, coherent back-scattering of a laser pulse from dense relativistic electron layers (mirrors), created by laser irradiation of nanometre-thin foils, has been theoretically and numerically analysed [16, 17].

In typical Compton scattering experiments the laser pulse and the e-beam are focused to a spot size of tens of micrometres in diameter. This relatively moderate focusing is typically compensated by using a high-power laser for a reasonable efficiency. The vast majority of Compton scattering experiments done so far employed *free-space* focusing, and this can be mathematically modelled as a Gaussian beam. In the framework of this representation, the Rayleigh length is proportional to the spot area, and therefore focusing the laser comes at the expense of reducing the length of interaction between the e-beam and the laser—which is approximately two Rayleigh lengths. However, *brightness* which is proportional to the local power density and *monochromaticity* which in turn is proportional to the interaction length are both essential qualities in many fields involving x-ray imaging. Therefore, compromising one at the expense of the other is of limited appeal, and a setup that facilitates both high-power density and long interaction is desirable.

2. Proposed paradigm—inverse Compton scattering in a Bragg structure

The easiest conceptual method to decouple focusing from interaction length is by introducing a *wave-guiding* structure. In this report we explore the possibility to leverage the previous

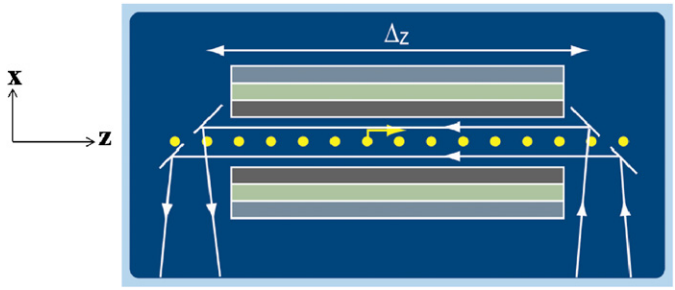

Figure 2. Proposed setup. Instead of free-space, the interaction between the e-beam and the laser will be inside an optical Bragg structure, capable of confining the laser light within a sub-micrometre hollow core. Proper design of the first 'matching' layer facilitates guiding a TEM mode within the core, which is optimal from the viewpoint of x-ray generation. Along with tight confinement, the interaction can be extended to the length of the waveguide itself, Δ_z, i.e. up to a centimetre scale, resulting in ultra-narrowband emission.

work done by our group, which proposes a special type of a hollow-core Bragg waveguide whose first layer (the layer adjacent to the hollow core) is different from the subsequent Bragg layers [18–20]. Such a Bragg waveguide can confine the light very efficiently to a *sub-wavelength* core, by properly designing this first 'matching' layer. This means that the laser cross section size is reduced by more than an order of magnitude compared with free-space configurations. The Bragg structure is shown to be able to support fields as high as $\sim$1 (GV m^{-1}) [18]. Additionally, the interaction can be as long as the waveguide itself, independently of the core size, implying that centimetre-scale interaction lengths are feasible, resulting in ultra-narrowband emission. As previous analysis shows [18, 19], by properly designing the Bragg layers, various properties of the guided mode can be achieved. Two of these properties are of interest for the process of inverse Compton scattering: (i) a TEM mode can be guided [19]. TEM mode is very important for Compton scattering, since it has no longitudinal field component that can potentially decelerate the e-beam, while transverse field components generate transverse e-beam oscillations similarly to undulators. The process of Compton scattering utilizing a TEM mode guided in a Bragg waveguide is schematically depicted in figure 2. Furthermore, in contrast to a free-space configuration, the field is uniform in the interaction region. (ii) TM_{01} mode with phase velocity c can be guided as well, with a different matching layer design [18]. This mode is optimal for e-beam *acceleration*, and it can replace the large RF linear accelerators used in current inverse Compton scattering experiments. The combined two-stage paradigm, the first stage being the acceleration of the e-beam by a co-propagating TM_{01} mode and the second stage being the inverse Compton scattering by a counter-propagating TEM mode, is shown in figure 3, and it introduces for the first time the prospect of a *table-top size bright and quasi-monochromatic* x-ray source.

2.1. Expected x-ray yield enhancement

Relying on a Bragg structure for a Compton scattering process will significantly improve the overall operation of an x-ray source by decoupling focusing and interaction length. In order to quantitatively assess the improvement, we now proceed to an analytical comparison between the two configurations: (i) Compton scattering based on free-space Gaussian beam, described in figure 1; (ii) Compton scattering in a Bragg structure, described in figures 2 and 3. For adequate comparison, we assume that both systems have the same e-beam characteristics and the laser injected into both systems is identical in terms of power and polarization (linear).

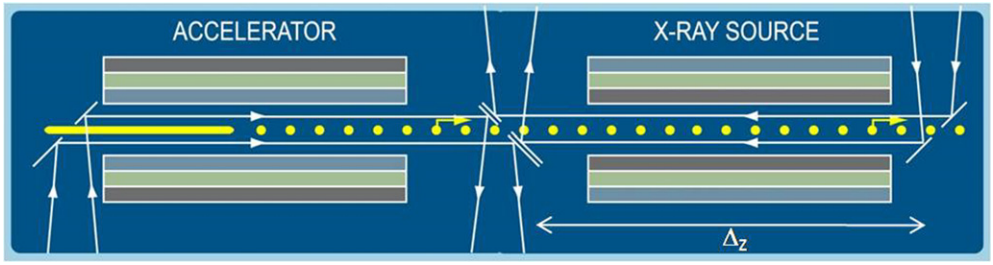

Figure 3. Proposed two-stage setup, the first stage being optical acceleration by TM_{01} mode guided in an optical Bragg accelerator. The second stage is inverse Compton scattering inside a Bragg structure with a different design, which is described in figure 2. This *table-top size* setup (from acceleration to emission) will be able to produce both bright and quasi-monochromatic x-rays.

For simplicity, we will make the comparison in a two-dimensional regime. This means that in both configurations the laser profile is focused along the x-axis only and is uniform along the y-axis (see figures 1 and 2 for definition of axes). This also implies that the e-beam shape is sheet-like instead of pencil-like, and so is the shape of the emitted x-ray. At the foundation of our comparison will be the following expression for the emitted number of photons and the energy, both per unit solid angle [1]:

$$\begin{aligned} \frac{\mathrm{d}N_{\mathrm{photons}}}{\mathrm{d}\Omega} &= \kappa^2 N_{\mathrm{electrons}} N_{\mathrm{opt}} \alpha_F \gamma^2 \frac{[1-(\gamma\theta)^2]^2 + 4(\gamma\theta)^2 \sin^2\phi}{[1+(\gamma\theta)^2]^4}, \\ \frac{\mathrm{d}W}{\mathrm{d}\Omega} &= \hbar\omega_{\mathrm{c}}(\theta,\gamma)\frac{\mathrm{d}N_{\mathrm{photons}}}{\mathrm{d}\Omega}; \qquad \omega_{\mathrm{c}}(\theta,\gamma) = \omega_{\mathrm{L}}\frac{4\gamma^2}{1+(\gamma\theta)^2}. \end{aligned} \tag{4}$$

Equation (4) is applicable in the weak interaction regime ($\kappa \ll 1$), in which moderate power inverse Compton sources operate. In fact, the proposed Bragg structure cannot operate above $\kappa \sim 8 \times 10^{-4}$, due to non-linear effects and surface damage caused by strong laser intensity. Therefore, the proposed Bragg setup is intended to be useful mainly within the field of *moderate* power inverse Compton sources. The typical deflection parameter of the Bragg structure is $\kappa = 3 \times 10^{-4}$, assuming electric fields of $\sim$1 (GV m^{-1}). $N_{\mathrm{electrons}}$ in equation (4) is the number of electrons in the e-beam. The fact that the overall x-ray yield in equation (4) is proportional to the number of electrons relies on the assumption that the emissions of different electrons are uncorrelated. This is indeed the case for all systems described in this study. N_{opt} in equation (4) is the number of optical cycles encountered by the electron traversing through the interaction region, and it is given by $N_{\mathrm{opt}} = 2\Delta_z/\lambda_{\mathrm{L}}$, where Δ_z is the length of the interaction region. The factor of 2 in $2\Delta_z$ is due to the fact that the laser and the e-beam are moving towards each other. $\alpha_{\mathrm{F}} \approx 1/137$ is the fine structure constant, ω_{L} is the laser angular frequency, θ and φ are the angular coordinates of the detector, θ being measured from the z-axis. ω_{c} is the central frequency of the emitted x-ray. The expression for ω_{c} in equation (4) is very precise for the Bragg case, but in a free-space Gaussian case a correction factor is required to account for the Gouy phase. Other than that, the only difference between the free-space and the Bragg configuration in equation (4) lies in the deflection parameter $\kappa = eE_0/mc\omega_{\mathrm{L}}$, E_0 being the effective (rms) electric field amplitude experienced by the electron in the interaction region, and it is very different in the two configurations. In the Bragg configuration, E_0 can be derived as

$$E_0^2 = 2 \times \frac{1}{\Delta_z}\int_{-\Delta_z/2}^{\Delta_z/2} \|\vec{E}\|^2 \mathrm{d}z \simeq \frac{2\eta_0}{D_{\mathrm{core}}}\chi\frac{P}{\Delta_y}, \tag{5}$$

$$\|\vec{E}\|^2 = \frac{2\eta_0}{D_{\mathrm{core}}}(\chi P/\Delta_y)\cos^2\left(2\pi\frac{ct}{\lambda_L} + 2\pi\frac{z}{\lambda_L}\right). \tag{6}$$

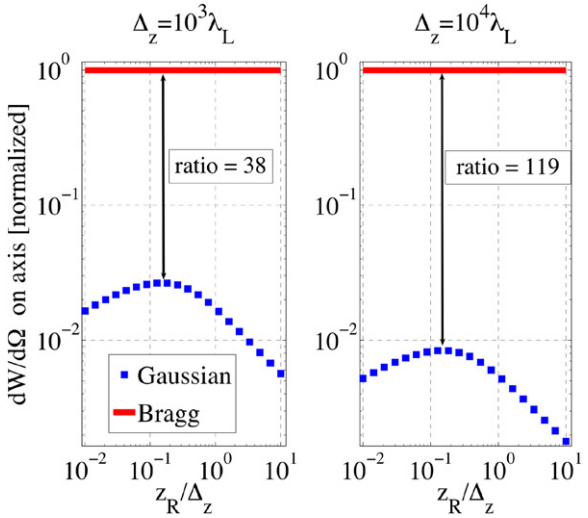

Figure 4. Comparison between the x-ray yield of an optical Bragg setup, described in figures 2 and 3, and the yield of the free-space configuration, described in figure 1. The yield enhancement is shown to exceed 38 in a millimetre long configuration and 119 in a centimetre long configuration (assuming $\lambda_L = 1\,\mu$m). The main reason for such enhancement is decoupling focusing and interaction length by introducing a wave-guiding structure. This destructive trade-off is graphically described by the blue (free-space) curve (squares): if z_R is too small, the interaction is too short, and if z_R is too large the focusing is too weak (in both cases the yield falls off).

P/Δ_y is the injected laser power per unit length in the y-direction. D_{core} is the width of the hollow core in Bragg structure. χ is the confinement factor of the Bragg structure indicating the percentage of the overall laser power that is actually located inside the core. In a well designed structure χ is quite high, but in order to be conservative we will assume $\chi = 0.5$; $\eta_0 \approx 377\Omega$ is the wave impedance in vacuum. The $2\times$ factor in equation (5) is because we are only interested in the field *amplitude*. In the Gaussian configuration, E_0 can be derived as

$$E_0^2 = 2 \times \frac{1}{\Delta_z}\int_{-\Delta_z/2}^{\Delta_z/2} \|\vec{E}(x=0)\|^2 \mathrm{d}z \cong \frac{4\eta_0}{\sqrt{2z_R\lambda_L}} \frac{\operatorname{arcsinh}\left(\frac{\Delta_z}{2z_R}\right)}{\frac{\Delta_z}{2z_R}} \frac{P}{\Delta_y}, \tag{7}$$

$$\|\vec{E}\|^2 = \frac{4\eta_0}{\sqrt{2z_R\lambda_L}} \frac{P}{\Delta_y} \frac{1}{\sqrt{1+(z/z_R)^2}} \exp\left[-\frac{2x^2/w_0^2}{1+(z/z_R)^2}\right] \times \cos^2\left[2\pi\frac{ct}{\lambda_L} + 2\pi\frac{z}{\lambda_L} + \frac{z_R}{z}\frac{x^2/w_0^2}{1+(z_R/z)^2} - \frac{1}{2}\arctan\left(\frac{z}{z_R}\right)\right], \tag{8}$$

where z_R is the Rayleigh length of the Gaussian beam and $w_0 = (z_R\lambda_L)^{1/2}/\pi$ is the spot radius. By substituting equations (5) and (7) into the definition of κ and then into equation (4) we are finally in a position to compare the emitted energy per unit solid angle in both configurations (comparison of the number of emitted photons leads to the same result). This comparison is shown in figure 4 for two interaction lengths Δ_z: $10^3\lambda_L$ (about 1 mm) and $10^4\lambda_L$ (about 1 cm). The free-space case exhibits an optimum at the Rayleigh length $z_R = 0.15\Delta_z$: for lower z_R the interaction is too short and for higher z_R the focusing is too weak, this being the graphic representation of the destructive trade-off existing in free-space configurations

Table 1. Typical values for the energy of the emitted photons and the x-ray bandwidth, assuming $N_{\mathrm{opt}} = 2 \times 10^3$, $\lambda_{\mathrm{L}} = 1\,\mu$m and $\gamma = 50$.

Electron energy (MeV)	5	10	25	250
Peak energy of emitted photons (keV)	0.5	1.9	11.9	1192
Bandwidth (FWHM) (eV)	0.2	0.8	5.3	528

between focusing and interaction length. This destructive trade-off is *nonexistent* in the Bragg structure, due to which enhancement of at least one order of magnitude can be achieved, as shown in figure 4. The minimal enhancement factor (at $z_{\mathrm{R}} = 0.15\Delta_z$) is given by equation (9):

$$\text{Minimal enhancement} = \frac{(\mathrm{d}W/\mathrm{d}\Omega)_{\mathrm{Bragg}}}{\max\limits_{z_{\mathrm{R}}}(\mathrm{d}W/\mathrm{d}\Omega)_{\mathrm{Gauss}}} = \frac{(E_0^2)_{\mathrm{Bragg,\ eq.\ (5)}}}{\max\limits_{z_{\mathrm{R}}}(E_0^2)_{\mathrm{Gauss,eq.\ (7)}}} = \frac{(E_0^2)_{\mathrm{Bragg}}}{[(E_0^2)_{\mathrm{Gauss}}]_{z_{\mathrm{R}}=0.15\Delta_z}}$$

$$= \chi\frac{\lambda_{\mathrm{L}}\Delta_z}{2.1D_{\mathrm{core}}}. \tag{9}$$

This simple analytical expression for the minimal enhancement provided by the Bragg structure is the main result of this study. For $\Delta_z = 10^3\lambda_{\mathrm{L}}$ the minimal enhancement is 38 and for $\Delta_z = 10^4\lambda_{\mathrm{L}}$ the minimal enhancement is 119. Both values are shown in figure 4.

3. Spectral linewidth of the emitted x-ray and requirements on the e-beam quality

As mentioned above, using the Bragg structure allows extending the interaction region to the centimetre scale, which is impossible to do with free-space focusing without almost completely defocusing the laser. This means that the number of electron oscillations during the interaction (N_{opt}) may exceed 10^4, which is very beneficial for a narrowband emission. The x-ray spectrum emitted by a *single* particle is given by equation (10):

$$\frac{\mathrm{d}^2W}{\mathrm{d}\omega\,\mathrm{d}\Omega} = \frac{\mathrm{d}W}{\mathrm{d}\Omega}\frac{N_{\mathrm{opt}}}{\omega_{\mathrm{c}}(\theta,\gamma)}\mathrm{sinc}^2\left[\pi N_{\mathrm{opt}}\frac{\omega-\omega_{\mathrm{c}}(\theta,\gamma)}{\omega_{\mathrm{c}}(\theta,\gamma)}\right],$$
$$\frac{\mathrm{d}W}{\mathrm{d}\Omega} \quad \text{and } \omega_{\mathrm{c}}(\theta,\gamma) - \text{from eq. (4)}. \tag{10}$$

A noteworthy fact emerging from equation (10) is that the FWHM *relative* bandwidth of the main lobe is on the order of $\delta\omega/\omega \sim 1/N_{\mathrm{opt}}$, which is independent of the e-beam acceleration (γ), while the *actual* bandwidth scales as γ^2. Table 1 gives some numerical examples for the bandwidth of the emitted x-ray.

In order to be able to benefit from this narrow bandwidth feature, enabled by the optical Bragg setup, the e-beam quality must be sufficiently high. There are two types of e-beam quality requirements. The first type is purely geometrical: the e-beam must be focused into a sheet with sub-micrometre thickness, small enough to fit in the waveguide core, and it must have small enough angular divergence in order to be able to pass through the narrow but long hollow core without hitting the inner walls of the waveguide. The maximal angular divergence in radians that can be tolerated from this point of view ($\delta\theta_{\mathrm{max}}$) is just the aspect ratio of the waveguide core: $\delta\theta_{\mathrm{max}} = D_{\mathrm{core}}/\Delta_z$ (on the order of 0.1 mrad). The second type of the e-beam requirements is spectral: fluctuations in kinetic energy (γ) among the electrons ('e-beam temperature') and e-beam angular spread can both significantly broaden the spectrum of the emitted x-ray, thus potentially cancelling the advantage of having a long interaction.

We will use equation (10) in order to quantify the limitations on the e-beam temperature and its angular spread. Even though the emission spectrum in equation (10) corresponds to

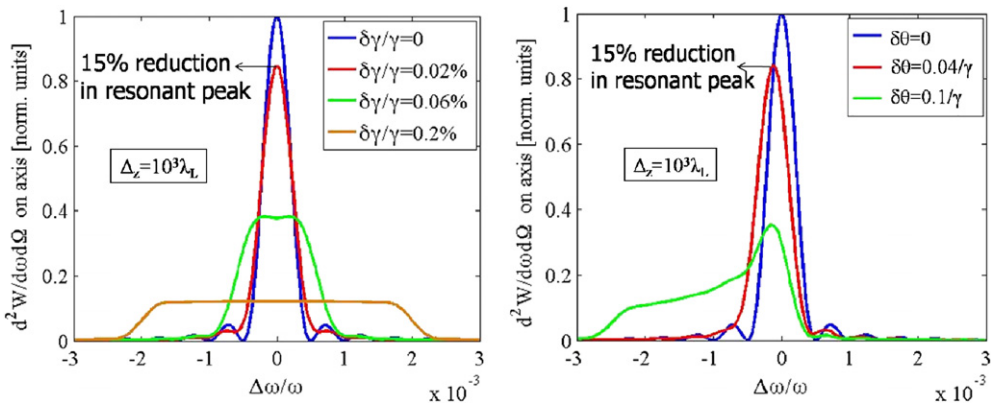

Figure 5. Spectral degradation of the emitted x-ray as a function of e-beam temperature ($\delta\gamma/\gamma$, left) and angular spread ($\delta\theta$, right). E-beam temperatures larger than $\delta\gamma/\gamma = 0.2\%$ and e-beam angular spreads larger than $\delta\theta = 0.04/\gamma$ are shown to cause significant broadening of the emission spectrum.

a single electron, the spectrum of the *entire e-beam* has the same shape as the single particle spectrum with one difference—the uncorrelated emissions of a large number of electrons introduce significant noise into the overall spectrum. Apart from this noise, the uncorrelated nature of emissions from different particles makes it easy to analyse the effect of e-beam temperature and angular spread, since a simple integration over equation (10) within the relevant range of angles and γ's gives an excellent approximation to the overall spectrum impaired by e-beam imperfections. The results are shown in figure 5, which reveals the undesired spectral broadening as a function of e-beam temperature and its angular spread. Evidently, an e-beam temperature of $\delta\gamma/\gamma = 0.02\%$ and angular spread of $0.04/\gamma$ radians are significant enough to affect monochromaticity. Figure 5 (right) also shows that the angular spread of the e-beam causes asymmetric broadening towards smaller frequencies. This is because off-axis electron trajectories in both $+x$ and $-x$ directions (positive and negative θ respectively) *reduce* the Doppler shift in the same way, whereby the maximal frequency corresponds to on-axis ($\theta = 0$) electron trajectories.

Among the two types of requirements on the e-beam angular spread, the geometric and the spectral, the geometric requirements are in fact more stringent. For example, assuming $\gamma = 50$, the angular spread requirement from the spectral point of view is $\delta\theta_{\max} = 0.04/\gamma = 0.8$ mrad, while the angular spread requirement from the geometric point of view is $\delta\theta_{\max} = 0.1$ mrad, as mentioned above. Current technology is capable of generating e-beams within these quality limits. However, the linear accelerators used for current inverse Compton experiments are about an order of magnitude above this requirement: $\delta\theta = 0.1/\gamma$ and $\delta\gamma/\gamma = 0.15\%$ [13], mainly because the linewidths in these experiments are broader than those discussed in this section, and therefore the requirements on e-beam quality are less stringent.

4. Achievable brightness

Another important figure of merit that characterizes the x-ray emission is spectral brightness, a formulation for which is given in equation (11):

$$B\left[\frac{\text{photons/sec}}{\text{mm}^2 \times \text{mrad}^2 \times 0.1\%\text{BW}}\right] = \overline{B}J\left[\frac{\text{mA}}{\mu\text{m}^2}\right]\eta_{\theta_x}\eta_{\theta_y} = 4.55 \times 10^{10}(\kappa\gamma N_{\text{opt}})^2\eta_{\theta_x}\eta_{\theta_y}. \quad (11)$$

Table 2. Properties of two recent state of the art inverse Compton scattering experiments.

	Peak spectral brightness $\left[\frac{\text{photons s}^{-1}}{\text{mm}^2\times\text{mrad}^2\times 0.1\%\text{BW}}\right]$	Emitted photon energy	Electron energy	Laser wavelength (nm)
KEK + BNL [22]	1.7×10^{18}	56 (MeV)	1.28 (GeV)	532
LLNL [21]	10^{17}	65 (keV)	56 (MeV)	815

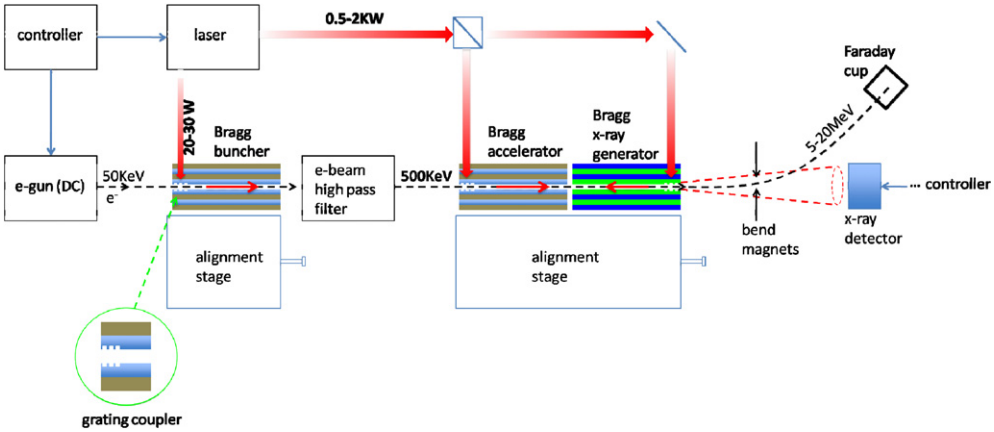

Figure 6. Conceptual schematic of the experimental setup (not to scale). Unlike most Compton experiments, linac and rf gun are replaced by their optical Bragg equivalent.

$\overline{B}$ in equation (11) is the normalized brightness per unit e-beam current density, J being the current density. We use the following reasonable parameters for the estimation of $\overline{B}$: $\kappa = 3.1 \times 10^{-4}$, $\gamma = 50$, $N_{\text{opt}} = 2 \times 10^4$. The current densities at the focal point achievable in current inverse Compton experiments are fairly high: on the order of $J = 100$ (mA μm^{-2}) [13, 21] as a result of various e-beam focusing techniques. We estimate that the same current density can be achievable in our setup. η_{θ_x} and η_{θ_y} in equation (11) are efficiency coefficients accounting for e-beam angular spreads along the x- and y-axes. They are given by $\eta_{\theta_i} = [1 + N_{\text{opt}}(\gamma\delta\theta_i)^2]^{-1/2}$, where i is either x or y. Assuming $\delta\theta_x \approx \delta\theta_y = 0.1$ mrad, according to the previous section, and $\gamma = 50$, we get efficiencies of $\eta_{\theta_x} \approx \eta_{\theta_y} \approx 82\%$, which amounts to a total angular efficiency of $\eta_{\theta_x}\eta_{\theta_y} \approx 67\%$. This brings the estimation of brightness to the order of 3×10^{17} (photons s^{-1} mm^{-2} mrad^{-2}/0.1%BW). This estimated brightness is comparable to the values achievable in current inverse Compton experiments, which use laser powers several orders of magnitude higher than in our proposed setup. The relevant data from two state of the art Compton scattering experiments are summarized in table 2.

5. Experimental setup

The conceptual schematics of an experimental setup for the Bragg x-ray generation experiment is shown in figure 6. Since the acceleration is mostly done by the Bragg accelerator, a simple dc electron gun which produces e-beams with initial relatively low kinetic energy of ~50 keV is sufficient for this setup. Prior to acceleration, the e-beam is focused into the narrow vacuum tunnel of the buncher consisting of a Bragg structure, which is virtually identical to the Bragg acceleration structure described above. The bunching is a consequence of the trapping of a fraction of the electrons in each optical period by the longitudinal component of the E-field.

The latter may be coupled into the Bragg structures using 90° grating couplers—see Zhang *et al* [23]. Electrons emerging from the buncher have a broad spectrum and for proper further acceleration the slow electrons are filtered out. Beyond this stage the high energy electrons are injected into the double-Bragg structure, described in figure 3. This double-Bragg structure will use laser power of 0.5–2 kW, corresponding to a deflection parameter of $\kappa \sim 3 \times 10^{-4}$. This laser power is thus significantly lower than in typical Compton experiments, due to the enhanced efficiency of the suggested paradigm. After the interaction, the x-ray is measured by a detector and the e-beam is collected by the Faraday cup. Not shown in the diagram are the electrons' optics. In contrast to regular acceleration structures made of metals, the Bragg acceleration structures are made of dielectrics. Therefore, electrostatic focusing will play a crucial role.

6. Conclusion

We have presented a new paradigm that is expected to improve by about two orders of magnitude the efficiency of x-ray generation by inverse Compton scattering. This efficiency enhancement is achieved by leveraging a uniquely designed optical Bragg structure, which facilitates sub-wavelength confinement combined with long interaction, extending up to a centimetre scale. Such a combination is impossible in free-space setups, in which focusing comes at the expense of interaction length. We have shown that our setup is expected to achieve brightness of 3×10^{17} (photons s^{-1} mm^{-2} $mrad^{-2}$/0.1%BW), which is comparable to current experiments, using only a fraction of injected laser power. The proposed concept imposes quality requirements on the e-beam, which are also discussed in this paper.

References

[1] Attwood D 2007 *Soft X-Rays and Extreme Ultraviolet Radiation: Principles and Applications* (Cambridge: Cambridge University Press)
[2] Allen P G, Perry D L, Mini S M and Stock S R 2001 *Applications of Synchrotron Radiation Techniques to Materials Science* vol 6 (Pittsburgh, PA: Materials Research Society)
[3] Burattini E and Balerna A 1996 *Biomedical Applications of Synchrotron Radiation* (Amsterdam: IOS Press)
[4] Sham T-K 2002 *Chemical Applications of Synchrotron Radiation* (Singapore: World Scientific)
[5] Onuki H and Elleaume P 2003 *Undulators, Wigglers, and their Applications* (Boca Raton, FL: CRC Press)
[6] Tsuji K, Injuk J and Grieken R 2004 *X-Ray Spectrometry: Recent Technological Advances* (New York: Wiley)
[7] Yorozu M, Yang J, Okada Y, Yanagida T, Sakai F, Ito S and Endo A 2003 *Appl. Phys. B: Lasers Opt.* **76** 293–7
[8] Kashiwagi S *et al* 2005 *J. Appl. Phys.* **98** 123302
[9] Babzien M *et al* 2006 *Phys. Rev. Lett.* **96** 054802
[10] Schwoerer H, Liesfeld B, Schlenvoigt H-P, Amthor K-U and Sauerbrey R 2006 *Phys. Rev. Lett.* **96** 014802
[11] Phuoc K T, Rousse A, Pittman M, Rousseau J P, Malka V, Fritzler S, Umstadter D and Hulin D 2003 *Phys. Rev. Lett.* **91** 195001
[12] Carmel Y, Granatstein V L and Gover A 1983 *Phys. Rev. Lett.* **51** 566
[13] Pogorelsky I V *et al* 2000 *Phys. Rev. ST Accel. Beams* **3** 090702
[14] Gibson D J *et al* 2004 *Phys. Plasmas* **11** 2857
[15] Bulanov S V, Esirkepov T and Tajima T 2003 *Phys. Rev. Lett.* **91** 085001
[16] Meyer-ter-Vehn J and Wu H-C 2009 *Eur. Phys. J.* D **55** 433
[17] Qiao B, Zepf M, Borghesi M, Dromey B and Geissler M 2009 *New J. Phys.* **11** 103042
[18] Mizrahi A and Schächter L 2004 *Phys. Rev.* E **70** 016505
[19] Mizrahi A and Schächter L 2004 *Opt. Express* **12** 3156
[20] Karagodsky V, Mizrahi A and Schächter L 2006 *Phys. Rev. ST Accel. Beams* **9** 051301
[21] Hartemann F V *et al* 2004 *Proc. EPAC 2004 (Lucerne, Switzerland)* p 270
[22] Sakai I *et al* 2003 *Phys. Rev. ST Accel. Beams* **6** 091001
[23] Zhang Z, Tantawi S G and Ruth R D 2005 *Phys. Rev. ST Accel. Beams* **8** 071302